

THE EFFECTS OF NON-GAUSSIAN INITIAL CONDITIONS ON THE STRUCTURE AND SUBSTRUCTURE OF COLD DARK MATTER HALOS

VLADIMIR AVILA-REESE AND PEDRO COLÍN

Instituto de Astronomía, U.N.A.M., A.P. 70-264, 04510, México, D.F., México

GABRIELLA PICCINELLI

Centro Tecnológico, ENEP Aragón, UNAM. Av. Rancho Seco s/n, Col. Impulsora, Cd. Nezahualcóyotl, México
AND

CLAUDIO FIRMANI

Osservatorio Astronomico di Brera, via E.Bianchi 46, I-23807 Merate, Italy

Subject headings: cosmology:dark matter — galaxies:formation — galaxies:halos — methods: N -body simulations

submitted to the *Astrophysical Journal*

ABSTRACT

We study the structure and substructure of halos obtained in N -body simulations for a Λ Cold Dark Matter (Λ CDM) cosmology with non-Gaussian initial conditions (NGICs). The initial statistics are lognormal in the gravitational potential field with positive (LN_p) and negative (LN_n) skewness; the sign of the skewness is conserved by the density field, and the power spectrum is the same for all the simulations. Our aim is not to test a given non-Gaussian statistics, but to explore the generic effect of positive- and negative-skew statistics on halo properties. From our low-resolution simulations, we find that LN_p (LN_n) halos are systematically more (less) concentrated than their Gaussian counterparts. This result is confirmed by our Milky Way- and cluster-sized halos resimulated with high-resolution. In addition, they show inner density profiles that depend on the statistics: the innermost slopes of LN_p (LN_n) halos are steeper (shallower) than those obtained from the corresponding Gaussian halos. A subhalo population embedded in LN_p halos is more susceptible to destruction than its counterpart inside Gaussian halos. On the other hand, subhalos in LN_n halos tend to survive longer than subhalos in Gaussian halos. The spin parameter probability distribution of LN_p (LN_n) halos is skewed to smaller (larger) values with respect to the Gaussian case. Our results show how the statistics of the primordial density field can influence some halo properties, opening this the possibility to constrain, although indirectly, the primordial statistics at small scale.

1. INTRODUCTION

The inflationary-motivated Cold Dark Matter (CDM) cosmology describes rather well a large body of observational data at large scales and has served as a useful theoretical framework for investigating galaxy formation and evolution (see for recent reviews e.g., Frenk 2002; Firmani & Avila-Reese 2003). In the CDM cosmology, the initial density fluctuation field is the starting point for calculating the structure formation in the universe. The simplest assumption for the statistical distribution of the primordial density fluctuations is the Gaussian one, which is valid only in the limit of zero fluctuation amplitude; for finite rms fluctuations, the Gaussian statistics assigns a non-zero probability to regions of negative density. In the context of simple inflationary models, the Gaussian distribution may arise in a natural fashion. However, as we will see below, deviations from Gaussianity are possible, in particular for more complicated models of inflation, while from the observational point of view the results regarding non-Gaussianity are controversial. Moreover, it may happen that the statistics depend on scale, so that measurements made at large scales are not necessarily representative of the small scale statistics. An interesting question to explore is how non-Gaussian initial conditions (NGICs) do affect cosmic structure formation at small scales. In this

paper, we are interested in particular in the effects of NGICs on the density profiles of galaxy- and cluster-sized CDM halos as well as on the substructure abundance in the halos.

Following, we present a short review of theoretical studies and observational constraints related to non-Gaussianity, as well as a brief discussion of previous numerical works on large-scale structure formation using NGICs.

1.1. *Generation of Non-Gaussian fluctuations*

In the context of inflationary models, non-Gaussian fluctuations would be the signature of non-linearities during inflation. For the simplest single scalar field models, the slow-roll conditions prevent non-Gaussian primordial fluctuations from developing significantly (Kofman & Linde 1987; Ortolan, Lucchin & Matarrese 1988; Matarrese, Ortolan & Lucchin 1989; Barrow & Coles 1990; but see Acquaviva et al. 2002, who suggest that non-Gaussianity may develop at second order calculation in cosmological perturbations). These constraints can be partially relaxed when special non-linear conditions such as a non-vacuum initial state for the inflaton (Martin, Riazuelo & Sakellariadou 2000; Gangui, Martin & Sakellariadou 2002) or a departure from scale invariance in the inflaton potential (Lesgourgues, Polarski & Starobinsky 1998; Salopek

1992) are introduced. Deviations from a scale invariant spectrum indeed can make the primordial non-Gaussianity non-negligible (Acquaviva et al.). There are some pieces of evidence that the measured matter power spectrum presents a peculiar behavior: a sharp peak or break at $k \approx 0.05h^{-1}\text{Mpc}$ (e.g., Einasto et al. 1997; Peacock 1997; Gaztañaga & Baugh 1998), an abrupt bending of the spectral index n_s at scales smaller than $k \approx 0.1h^{-1}\text{Mpc}$ (Peacock 1997), and/or a running n_s from $n_s > 1$ at large scales to $n_s < 1$ at small scales (Peiris et al. 2003).

However, significant deviations from Gaussianity are more probable to occur in multi-field inflationary models. In this case, the deviations are produced by fluctuations of the field that does not drive inflation, and it is consequently not constrained by a flat potential. Generically, one gets a mixture of adiabatic and isocurvature perturbations, quadratic in a Gaussian field (e.g., Allen, Grinstein, & Wise 1987; Peebles 1999; Antoniadis, Mazur, & Motola 1997; Linde & Mukhanov 1997). In some proposals, the mixing between adiabatic and isocurvature modes may effectively transfer the non-Gaussian features from one sector to the other, rendering them more significant (Gordon et al. 2001, and references therein; Bernardeau & Uzan 2002; Bartolo, Matarrese & Riotto 2002). An overview of the characteristics and limitations of the non-Gaussian contributions in the different inflationary models, either with a single or with several scalar fields is presented by Bernardeau & Uzan.

A recently proposed alternative scenario consists in adiabatic density perturbations which originate after inflation from the perturbation of a field that is not the inflaton, and does not dominate the dynamics, the so called *curvaton* (Lyth & Wands 2002; Lyth, Ungarelli & Wands 2003; see also Linde & Mukhanov 1997; Moroi & Takahashi 2001, 2002). The perturbation is initially of the isocurvature type but, if the curvaton is long-lived, its energy density will have a relative increase with respect to radiation, and will finally generate a curvature perturbation. The curvaton scenario can generate significant non-Gaussianity since the curvature perturbation is proportional to the perturbation in the curvaton energy density, which is in turn a linear combination of the curvaton-field perturbation and its square. In this model, large isocurvature perturbations, correlated with adiabatic perturbations, may arise in dark matter and baryonic matter.

In contrast, in the topological-defect model, strong non-Gaussian (skew-positive) fluctuations in the density field rather than in the potential field may develop (e.g., Turok & Spergel 1990; Avelino, Shellard, & Wu 1998). Although this model has proved to be inconsistent with observations (e.g., Pen, Seljak & Turok 1997; Durrer, Kunz & Melchiorri 1998; Allen et al. 1997), a mixed model of inflation plus certain defects (cosmic strings and any other kind of global defects) seems to be still allowed by observations (Bouchet et al. 2002; Sakellariadou 2002 and references therein).

1.2. Observational constraints

As it has been just discussed, the theoretical prediction of the exact amplitude and precise form of non-Gaussianity in inflation is still an open question. Thus, we should turn to observations to look for its signatures and constraints (see Kamionkowski 2003 for a recent review on the sub-

ject). Care must be taken in drawing conclusions about the Gaussian nature of the density field from observations; the uncertainty in the measurements and the limited coverage of present observations can hide cosmological non-Gaussian features. We should also be aware that the gravitational evolution and some systematic effects introduce non-Gaussian signatures in an intrinsically Gaussian distribution. We also would like to stress that there are no *a priori* strong arguments to postulate that the statistics of the primordial fluctuations should be the same at all scales.

The most direct way to search for primordial non-Gaussianity (at large scales) is the Cosmic Microwave Background Radiation (CMBR). Many tests applied to the CMBR data resulted nearly consistent with Gaussianity (see e.g., Kogut et al. 1996, and Bromley & Tegmark 2000, and references therein, for COBE DMR maps; Polenta et al. 2002 for BOOMERanG maps; Santos et al. 2002, and Wu et al. 2001 for MAXIMA maps; Park et al. 2001 for QMAP and Saskatoon maps; Komatsu, et al. 2003 for WMAP results). However, non-Gaussian statistics have no generic signatures on the sky and different tests and data analysis, at different scales, may be better or worse suited for different types of non-Gaussian statistics. Therefore, it is important to consider carefully any new result that supports the possibility of non-Gaussian features using different techniques and indicators (e.g., Ferreira, Magueijo & Górski 1998; Magueijo 2000; Pando, Valls-Gabaud & Fang 1998; Chiang et al. 2003). Notice that Banday, Zaroubi, & Górski (2000) have shown that the non-Gaussian signal detected in the COBE data by Ferreira et al. was probably due to a systematic period in the COBE satellite flight —the “eclipse period”. See also Barreiro et al. (2000) for some comments on the other mentioned works.

The difficulty of predicting the precise form of non-Gaussianity from inflation or other seed mechanisms, led to define and work with some parametric indicators of the deviation from Gaussianity in a generic model instead of trying to look for a particular statistics. An often employed indicator is the non-linear coupling parameter f_{NL} that parameterizes the leading order non-linear/non-Gaussian correction to the primordial gravitational potential: $\Phi = \phi_L + f_{\text{NL}}[\phi_L^2 - \langle \phi_L^2 \rangle]$, where ϕ_L is a Gaussian random field. A similar definition is introduced for non-Gaussianity in the density field (see e.g., Verde et al. 2000). The recent first-year WMAP observations (processed with two statistics: the angular bispectrum and Minkowski functionals) have constrained f_{NL} in the range $-58 < f_{\text{NL}} < 134$ (95%) (Komatsu, et al. 2003). As a reference, let us recall that in some non-standard inflationary models, as the multi-field ones, f_{NL} can be as big as ~ 20 (Verde 2001), while in the single-field models with some non-linearities, $|f_{\text{NL}}| \lesssim 1$ (Acquaviva et al. 2002). Combining WMAP data with ACBAR, 2dF, and HST results, strong constraints can be obtained in specific cases of correlated primordial and adiabatic density fluctuations, such as curvaton models (Gordon & Lewis 2002).

Tegmark, de Oliveira-Costa & Hamilton (2003) have performed an independent foreground analysis from the WMAP data. Their foreground-cleaned and Wiener-filtered maps were used by Chiang et al. (2003) for a non-Gaussianity test. These authors implement a phase-

mapping technique (Chiang, Coles & Naselsky 2002), which has the advantage of testing non-Gaussianity at separate multipole bands (angular scales). A multipole band which is considerable non-Gaussian could have an insignificant non-Gaussian contribution to the whole map and produce thus an overall Gaussian realization. The authors show that the foreground-cleaned map is against Gaussianity at all 4 multipole bands centered around $\ell = 150, 290, 400$, and 500 . The Wiener-filtered map, on the other hand, is Gaussian for $\ell < 250$ ($\gtrsim 180h^{-1}\text{Mpc}$) but non-Gaussian for $\ell > 350$ ($\lesssim 50h^{-1}\text{Mpc}$). As it was said above, the statistics might change with the scale.

The effects of primordial non-Gaussianity can be also studied in the distribution of mass in the Universe (intermediate scales). The gravitational evolution not only amplifies the primordial density fluctuation field but also makes it non-Gaussian due to clustering. However, the non-Gaussianity generated by gravitational evolution can be calculated and subtracted from the present statistics (e.g., Verde et al. 2000). Some of the tests of non-Gaussianity include the abundance and distribution of galaxy clusters and galaxies, the evolution of these abundances, and the size-temperature relation of galaxy clusters.

Since galaxy clusters form at the highest density peaks, which are most sensitive to deviations from Gaussianity, their abundance, and in particular the evolution of their abundance, can be used to probe the statistics. A density distribution with positive (negative) skewness leads to more (less) high density peaks. In this field, a useful indicator of the amount of deviation from Gaussianity is the probability of obtaining a peak of height 3σ or higher (at a given “filtered” scale) for a certain statistics relative to the Gaussian one:

$$G_3 = 2\pi \frac{\int_3^\infty P(y)dy}{\int_3^\infty e^{-y^2/2}dy}. \quad (1)$$

Robinson, Gawiser & Silk (2000), and Koyama, Soda & Taruya (1999) (see also Chiu, Ostriker & Staruss 1998; Willick 2000) constrain primordial non-Gaussianity through the evolution of cluster abundance. They use a Press-Schechter formalism extended to NGICs for predicting cluster abundances at different redshifts and for different cosmological models. Koyama et al., using data sets at $z = 0$ and $z \sim 0.6$ for cluster abundance and the correlation length from the APM survey, obtained the upper bound $\Omega_m < 0.5$ and the lower bounds $G_3 > 2$ and $\sigma_8 > 0.7$ for a χ^2 non-Gaussian distribution; in particular for $\Omega_m = 0.3$ and $\Omega_\Lambda = 0.7$, non-Gaussianity of the order of $G_3 \sim 4$ (skew positive) is favored. Robinson et al. (2000), from several samples of clusters at redshifts between 0.05 and 0.8, find that for $\Omega_m = 0.3$, Gaussianity is consistent with the data, but a wide range of non-Gaussian lognormal models also fit the data, with values of $G_3 < 4$ ($G_3 < 6$ when including cosmological constant) acceptable at the 2σ level. It must be stressed that current constraints are not conclusive due to the difficulty in the determination of the mass of high-redshift clusters.

A long non-Gaussian tail would give not only an enhanced cluster abundance, but also a larger scatter in the formation redshifts and sizes of clusters with a given mass. A skew-positive distribution implies that halos collapse

during a broader range of redshifts than in the Gaussian case, leading to a larger scatter of clusters properties, such as size and temperature. Verde et al. (2001a) find that the predicted scatter for Gaussian initial conditions is consistent with the observed one and constrain G_3 to be $\lesssim 4$.

Galaxies at high redshift are another kind of rare objects in the universe, so their abundance is considered for testing non-Gaussianity by Verde et al. (2001b). Results are still very preliminar and uncertain. On the other hand, the bispectrum of the galaxy distribution from 2dF (Verde et al. 2002) and from SDSS (Szapudi et al. 2002) surveys have been found consistent with Gaussian initial conditions.

Finally, the statistics of large-scale galaxy clustering can also be used to constrain non-Gaussianity. Most of the previous cosmological numerical simulations with NGICs were aimed at studying precisely galaxy clustering. In the next subsection we review some of these works. In the present paper, we will introduce a new potential test for cosmological models with NGICs at the smallest scales, by exploring the inner structure and substructure of the dark matter halos.

1.3. Previous numerical works

In an attempt to overcome the problem of lack of power at large-scales of the standard CDM cosmology, among other alternatives, models with NGICs were proposed and tested by means of N-body simulations. Moscardini et al. (1991, hereafter MMLM; see also Messina et al 1990) constructed certain multiplicative non-Gaussian statistics for the peculiar gravitational potential, and used them as initial conditions of N -body cosmological simulations. The outcome of the simulations were analyzed by different statistical tests at large-scales and compared with observations. It was found that both the clustering dynamics and the present day texture are mostly sensitive to the sign of the initial skewness of density fluctuations. Positive models cluster to a lumpy structure with small coherence length, while negative models build up a cellular structure with large coherence length, large voids, and enhanced peculiar motions. In a subsequent paper, the same authors showed that some relevant differences may appear for models with the same sign of the skewness but different statistics (Coles et al. 1993). For example, they showed that their CDM skew-negative χ^2 model agrees rather well with the 2D topology inferred from the Lick Catalogue, while the skew-negative lognormal model (as well as the skew-positive models) give discrepant results. From the analysis at smaller scales, Matarrese et al. (1991) found that groups in skew-negative models are preferentially loose systems, slightly biased over the background, with high velocity dispersion and clear signal alignment with neighboring groups. Groups in skew-positive models are highly biased compact systems with lower velocity dispersion. In general, in the series of papers mentioned above, the authors concluded that standard CDM skew-negative models (predominance of primordial underdense regions) retain the advantages of the Gaussian biased standard CDM counterpart, and improve on several of their problems.

An extensive numerical study of the influence of NGICs on large-scale structure formation has been done also by Weinberg & Cole (1992). These authors attempted to isolate the effects of NGICs from other factors by con-

sidering a range of power-law power spectra and different cosmological models. Similar to Matarrese et al. (1991), they found that skew-positive models form structure by accreting mass onto rare high peaks, leaving large volumes almost unperturbed, while skew-negative models develop structures rich in expanding voids, sheets and filaments. The authors conclude that skew-positive models produce unrealistic large-scale features, while skew-negative models create attractive structure but, for the low-density universe ($\Omega_m = 0.2$) cluster velocity dispersions are too low and the voids are probably excessively large.

It should be noted that since the time these works appeared (early 90's), deep progresses in the determination of the cosmological parameters, the observational data on galaxy clustering, and the computational capability were made. Time is ripe to explore the effects of NGICs on structure formation by means of high-resolution N -body simulations for the preferred (concordance) cosmological model. This paper presents by first time a numerical study about the structure of halos formed under NGICs.

In §2 we present the non-Gaussian models to be used here, while in §3 the implementation of the NGICs in the N -body code is described and the different low- and high-resolution runs are presented. In §4.1, the halo concentrations and density profiles for the non-Gaussian and Gaussian runs are presented and compared among them. The spin parameter distribution of the low-resolution halos and the angular momentum distribution of the high-resolution halos is analyzed in §4.2. The ellipticity of the latter halos is analyzed in §4.3. In §4.4, results on the subhalo population in the galaxy and cluster halos are presented. The summary and the discussion are given in §5.

2. NON-GAUSSIAN MODELS

Since there is no preference for any particular non-Gaussian statistics (§1.1), we chose arbitrary non-Gaussian models. Our main interest is to study generically the influence of skew-positive and -negative NGICs on halo properties. To get the initial conditions for our simulations, we have followed closely MMLM, who constructed the non-Gaussianity in the gravitational potential fluctuation field, Φ , instead of the density field. The potential fluctuation Φ is related to the linear mass fluctuation via the Poisson equation. We first generate a Gaussian realization in Fourier space of a w random field with the primordial (scale-invariant) power spectrum

$$P_w(k) = Bk^{-3}, \quad (2)$$

where k is the comoving wave number, and B is the normalization factor. The zero-mean Gaussian field w is obtained in configuration space by inverse-Fourier transforming $\tilde{w}(\mathbf{k})$. The non-Gaussian field for the perturbations in the potential, $\Phi(\mathbf{x})$, is then built as the convolution of a real function $\tau(\mathbf{x})$ with a stationary, zero-mean random field $\phi(\mathbf{x})$, which is obtained from a non-linear transformation of the $w(\mathbf{x})$ Gaussian field. For a lognormal statistics the relation between w and the primordial potential fluctuation ϕ is given by

$$\phi(\mathbf{x}) = A \left[e^{w(\mathbf{x})} - \langle e^w \rangle \right], \quad (3)$$

where A is a normalization factor, related to B in eq. (2). The Fourier transformed of the function $\tau(\mathbf{x})$ is the

transfer function $T(k)$ used to get the processed power spectrum at the recombination epoch. The Fourier transformed function $\tilde{\Phi}(k)$, which is simply given by the product of $\tilde{\phi}(k)$ with $T^2(k)$, is subsequently processed by the Zel'dovich approximation algorithm.

Different lognormal statistics are obtained depending on the amplitude of the w Gaussian field. Although MMLM set $\langle w^2 \rangle = 1$, we prefer to assume a variance slightly smaller than one because it reproduces better the theoretical Λ CDM-density power spectrum. There is still freedom in choosing the sign of the constant A in eq. (3), with the sign determining the direction of the skewness. Our Gaussian realizations are also implemented using a ϕ field but in this case

$$\phi(\mathbf{x}) = Aw(\mathbf{x}). \quad (4)$$

We notice that because Gaussian models with opposite signs give rise to different realizations in a statistical sense, we had to simulate for each lognormal skew-positive LN_p or lognormal skew-negative LN_n model the corresponding gaussian G_p or G_n model. We also notice that because in general a statistical distribution for the gravitational potential does not imply the same distribution for the density field (MMLM), we should not expect the statistics of the density field to be lognormal, nevertheless the sign of the skewness is preserved.

In order to compute the probability distribution function (PDF) for the different statistics at the initial time $z_i = 50$ (after the application of the Zel'dovich approximation), our $100h^{-1}\text{Mpc}$ box simulation (see below) was divided in 64^3 cells. The density in each cell was then computed using the cloud-in-cell scheme. The skewness parameter $\xi \equiv \langle \delta^3 \rangle / \langle \delta^2 \rangle^{3/2}$ is 0.52, 3.90, and -1.27 for the Gaussian, LN_p and LN_n statistics, respectively, while the G_3 parameter defined in eq. (1) is 3.05 for LN_p and 0.067 for LN_n . Note that at z_i the PDF of the density field of a Gaussian realization is not Gaussian; in fact, we found that the PDF could be fitted by a lognormal, skew-positive, distribution: non-linear modes appear as a result of the application of the Zel'dovich approximation. This is why the skewness of the density field in the Gaussian scenario is not zero anymore.

3. NUMERICAL SIMULATIONS

The Adaptive Refinement Tree (ART) N -body code (Kravtsov, Klypin, & Khokhlov 1997) in its multiple-mass version was used to run a series of simulations aimed mainly at studying the structure of halos under different statistics. The ART code achieves high spatial resolution by refining the base uniform grid in all high-density regions with an automated refinement algorithm. The multiple-mass scheme is used to increase the mass and spatial resolution in few selected halos and its implementation is described in detail elsewhere (Klypin et al. 2001). All N -body simulations were performed in a low-density flat Λ CDM model with the following parameters: $\Omega_m = 0.3$, $\Omega_\Lambda = 0.7$, and $h = 0.7$. The power spectrum was normalized to $\sigma_8 = 1.0$, where σ_8 is the *rms* mass fluctuation in spheres of radius $8h^{-1}\text{Mpc}$ (the top-hat window is used).

As a test of our method for generating NGIC's, we first ran two simulations under G_p and LN_p statistics in a box of $20 h^{-1}\text{Mpc}$ for each side and 64^3 particles. Halos from

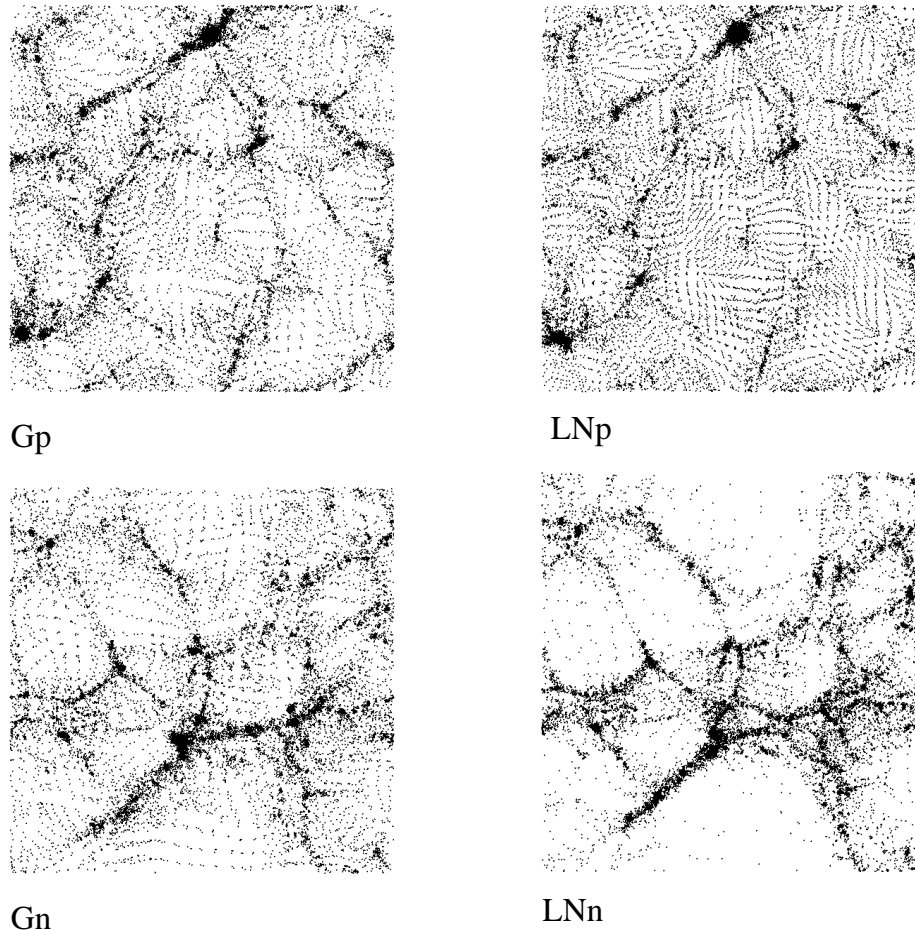


FIG. 1.— Projected particle positions in slices of one tenth the size of the $100 h^{-1}\text{Mpc}$ box at $z = 0$. Each slice contain about 26,000 dark matter particles. We note that the particle distributions are compared *at the same cosmological time* and not when the clustering properties of the different scenarios are comparable, as has often been the case in the literature (e.g., MMLM). Although, the differences in the large-scale pattern between a lognormal realization and its Gaussian counterpart are not as striking as they were compared *at the same clustering epoch*, we do see some differences: voids are emptier and more defined in the LN_n than in their Gaussian scenario. On the contrary, in the LN_p scenario voids are not as developed (they contain more DM particles) as in the Gaussian one.

these simulations were also used for further analysis. We also ran two simulations with low-mass resolution in boxes of 12.5 and $100 h^{-1}\text{Mpc}$ on a side. We selected, for resimulation with high-mass resolution and for each statistics, two galaxy-sized halos from the $12.5h^{-1}\text{Mpc}$ box and one cluster-sized halo from the $100h^{-1}\text{Mpc}$ box. In an attempt to study galaxy-sized halos with different mass assembly histories (MAHs), we simulated with high resolution two halos, $G1$ and $G2$, with different concentrations since it is known that the concentration of the halo is related to its MAH (Avila-Reese et al. 1998, 1999; Wechsler et al. 2002). We notice, however, that in a box as small as the one we chose for the search of galaxy-sized halos, only two or three halos can be found to satisfy simultaneously the following criteria: (a) comparable mass, (b) extreme concentrations, (c) isolation, and (d) with a counterpart

in the corresponding lognormal realization. Halos $G1_{\text{GP}}$ and $G2_{\text{GP}}$, for example, obey roughly these rules. They have masses that differ by a factor of three and NFW (Navarro, Frenk & White 1997; Eke, Navarro & Steinmetz 2001) concentrations, c_{vir} , of 16.4 and 11.4, for $G1_{\text{GP}}$ and $G2_{\text{GP}}$, respectively. The reason why we did not find a galaxy-sized halo with a very low concentration is because very often these halos are found accompanied with halos of comparable mass. In the rare case in which we do find an isolated halo with a low c_{vir} , it turns out to be too small or to lack a “partner” in the lognormal statistics.

The bound density maxima (BDM) group finding algorithm (Klypin & Holtzman 1997) was used to locate halos and subhalos in all simulations. The BDM algorithm identifies positions of local maxima in the density field at the scale of interest and applies physically motivated criteria

TABLE 1
SIMULATION PARAMETERS

statistics	L_{BOX} ($h^{-1}\text{Mpc}$)	m_p ($h^{-1}M_\odot$)	Resolution ($h^{-1}\text{kpc}$)	M_{vir} ($h^{-1}M_\odot$)	v_{max} (kms^{-1})	$c_{1/5}$	λ' (10^{-2})	Halo name tag
G_p	100.0	5.0×10^9	3.0	6.2×10^{14}	1407	6.1	2.82	Cl_{Gp}
LN_p	100.0	5.0×10^9	1.5	8.3×10^{14}	1643	7.2	1.37	Cl_{LNp}
G_n	100.0	5.0×10^9	3.0	1.6×10^{14}	913	6.8	3.79	Cl_{Gn}
LN_n	100.0	5.0×10^9	6.1	1.3×10^{14}	781	5.2	1.22	Cl_{LNn}
G_p	12.5	9.7×10^6	0.2	6.9×10^{11}	188	11.1	1.52	$G1_{Gp}$
G_p	12.5	9.7×10^6	0.2	2.3×10^{12}	241	8.0	1.22	$G2_{Gp}$
G_n	12.5	9.7×10^6	0.2	2.3×10^{12}	175	9.2	5.32	$G1_{Gn}$
G_n	12.5	9.7×10^6	0.2	2.8×10^{12}	253	7.8	3.13	$G2_{Gn}$
LN_p	12.5	9.7×10^6	0.1	3.0×10^{11}	303	19.5	2.03	$G1_{LNp}$
LN_p	12.5	9.7×10^6	0.2	2.1×10^{12}	256	9.3	0.69	$G2_{LNp}$
LN_n	12.5	9.7×10^6	0.4	7.3×10^{11}	157	7.0	6.15	$G1_{LNn}$
LN_n	12.5	9.7×10^6	0.4	2.7×10^{12}	218	5.1	10.00	$G2_{LNn}$

to find out whether a group of particles forms a gravitationally bound halo.

An overview of some of the characteristics of the studied halos are shown in Table 1. The symbol with which we denote the statistics is shown in column (1). The mass of the least massive particle is shown in column (3). It is only a function of the size of the box (col. [2]) because the cosmological model and the number of mass species are fixed. Column (4) shows the formal force resolution, measured by the size of a cell in the finest mesh. In general, the lognormal skew-positive (skew-negative) simulations have a higher (lower) resolution than the Gaussian counterparts because simulated halos in the former case reach a higher (lower) central density than in the latter one. The mass M_v within the virial radius, defined as the radius at which the average halo density is Δ_c times the background density according to the spherical top-hat model, is shown in column (5). Δ_c is a number that depends on epoch and cosmological parameters (Ω_m, Ω_Λ); for a flat Λ CDM model, $\Delta_c \sim 337$ at $z = 0$, where z is the redshift. The maximum circular velocity defined as

$$v_{\max} = \left(\frac{GM(< r)}{r} \right)_{\max}^{1/2}, \quad (5)$$

where G is the gravitational constant and $M(< r)$ is the mass contained within the radius r , is placed in column (6). In column (7) we show the $c_{1/5}$ halo concentration parameter (see §4.1). The spin parameter λ' as defined by Bullock et al. (2001) is shown in column (8) (see §4.2). In column (9) we introduce the halo name tag for each one of the simulated halos. Cluster- and galaxy-sized halos are named Cl_x and Gn_x , respectively, where x denotes the statistics and n the halo number.

4. RESULTS

Figure 1 shows projected particle positions at $z = 0$ from the $100h^{-1}\text{Mpc}$ box low-resolution simulations in slices of one-tenth of the box size. The differences in the particle distribution between the lognormal realizations and

the Gaussian ones are clearly seen: the density distribution in the LN_p statistics is lumpier with concentrated isolated peaks and a smaller coherence length, while in the LN_n statistics it has a cellular structure with bigger voids and a larger coherence length. Notice that the void population is different in both cases; for the LN_p model it appears to be larger than in the Gaussian case, while the contrary happens in the LN_n model. The contrasts among the different particle distributions are not as remarkable as shown, for example, in MMLM because of the different normalizations: we normalize our models to the same σ_8 while MMLM stop their simulations when “the particle two-point function is best fitted by a power law $\xi(r) = (r/r_0)^{-\gamma}$, with $\gamma = 1.8$, in a suitable interval”; accordingly, their LN_p (LN_n) models are less (more) evolved. We measured $\xi(r)$ at $z = 0$ for our different statistics and found, as expected, similar correlation length r_0 (defined as the radius r where $\xi(r) = 1$) values. However, for $r < r_0$ the correlation functions of the different scenarios start deviating from each other, with the greatest differences found at the smallest scales. As expected, the ξ functions of the LN_p , G_p (or G_n) and LN_n statistics are on the top, middle, and bottom, of the ξ vs. r diagram, respectively. In any case, it is not the aim of this paper to explore the large-scale structure produced in simulations with NGICs, but to explore the effects of NGICs on the properties of CDM halo.

Following, we present a study of the structural properties of galaxy- and cluster-sized halos from the non-Gaussian realizations and their comparison with the corresponding halos of the Gaussian simulations.

4.1. Concentrations and Density Profiles of Halos

In Figure 2 we show several general concentration parameters (vs. the halo mass M_h) measured for the halos in the low resolution simulations (12.5, 20 and $100 h^{-1}\text{Mpc}$ box size). These plots give us a preliminar idea of the effects of NGICs on the halo properties for a relatively large number of objects.

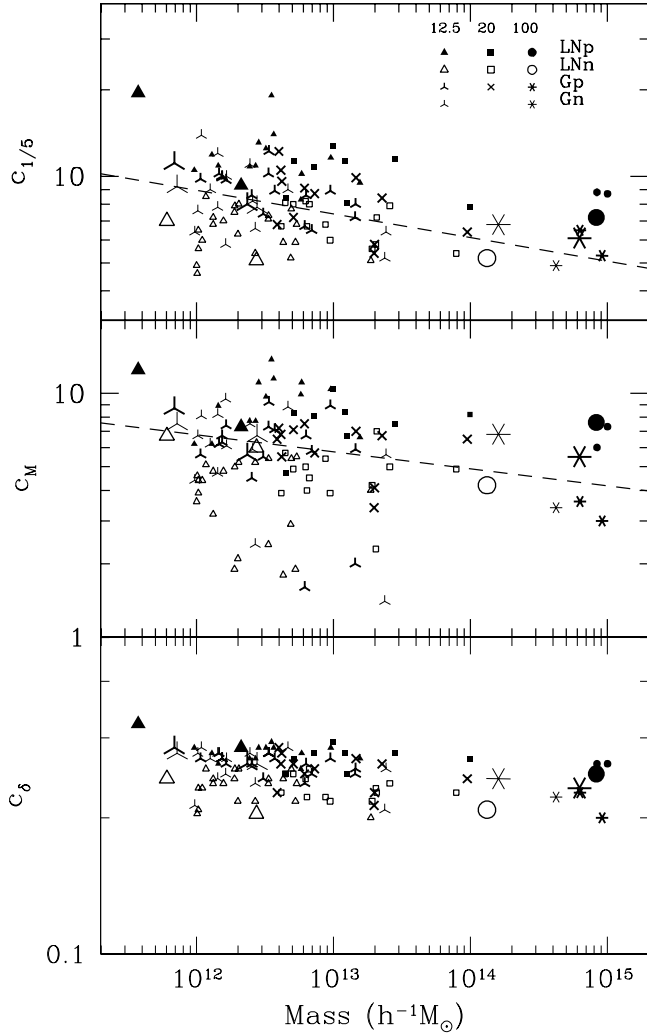


FIG. 2.— Different concentration parameters (see text) vs. M_v for the halos in the low-resolution simulations (small symbols) and those re-simulated with high-resolution (large symbols). Only halos with more than 1500 particles are plotted. The different symbols indicate the box size and the statistics of the simulations (see the legends in the upper panel). The dashed lines in the upper and medium panels are the linear fitting to the data (Gaussian isolated halos) presented in Avila-Reese et al. (1999), and the analytical estimate of c_M assuming the NFW profile and using $\log c_{\text{vir}} = 2.35 - 0.1 \log(M_v/h^{-1}M_\odot)$. According to each one of the three concentration parameters used, the LN_p (solid symbols) and LN_n (open symbols) halos are systematically more concentrated and less concentrated than the Gaussian halos (skeletal symbols), respectively.

Only halos with more than 1500 particles are plotted. The $c_{1/5}$ concentration (upper panel) is defined as the ratio between the halo radius (virial or truncation radius¹) and the radius where is contained one-fifth of the halo mass (Avila-Reese et al. 1999). This parameter depends on the definition and determination of the halo radius and mass. It is convenient to introduce other concentration

parameters that do not depend on these definitions. Here we use the c_M and c_δ parameters. The c_M concentration (medium panel) is defined as 27 times the ratio between the mass at $r_{\text{in}} = 8.5$ kpc ($v_{\text{max}}/220\text{kms}^{-1}$) and the mass at $r_{\text{out}} = 3 \times r_{\text{in}}$ (Davé et al. 2001). The c_δ concentration (lower panel) is defined as the ratio between the radius where the halo mean overdensity is 3×10^4 and where it is 800. The faster the density between these two radii decays (larger concentration), the larger is c_δ , tending to 1 in the limit. Notice that c_M traces the halo concentration in the inner region, while c_δ refers to a large portion of the halo, it is more global than c_M . We do not use the more common NFW concentration parameter, c_{vir} , because we do not know *a priori* whether the non-Gaussian halos will be described by the NFW density profile.

It is clear from Figure 2 that halos produced in the LN_p model are systematically more concentrated than the Gaussian ones, while the LN_n halos show an opposite trend. The LN_p halos from the different box realizations are plotted with solid symbols, while those from the LN_n simulations are plotted with open symbols. The corresponding Gaussian halos are plotted with skeletal symbols. Dashed lines are the expected values for NFW CDM halo. In the case of $c_{1/5}$ we take the results reported in Avila-Reese et al. (1999) for the isolated halos, while for c_M we use its numerical relations with c_{vir} , where for c_{vir} we took their average values in function of M_v as measured in the Gaussian ΛCDM simulation studied in Avila-Reese et al. (1999): $\log c_{\text{vir}} = 2.35 - 0.10 \log(M_v/h^{-1}M_\odot)$

Now we turn to the re-simulated halos with high-resolution. Their concentrations are also shown in Fig. 2 with the corresponding large symbols. Figure 3 shows their density profiles. Upper and lower panels are for the skew-positive and skew-negative models, respectively. Left and medium columns are for the high- and low-concentrated galaxy-sized halos, respectively, and right column is for the single cluster-sized halo. The LN -model halo profiles are plotted with solid lines, while the corresponding Gaussian-model halo profiles (calculated with the same seed) are plotted with dashed lines. The dotted lines are the NFW fitting to the Gaussian halos; the fittings are satisfactory, excepting at the very inner regions where the halo profiles are slightly steeper than the NFW profile, in particular for the halos in the lower panels. As said in §2.2, we selected two different galaxy-sized halos from the low-resolution simulation in order to cover the intrinsic (cosmological) dispersion on halo structures, which is mainly due to the dispersion on the halo mass aggregation histories, given on its own by the statistical nature of the primordial density fluctuation field.

The results presented in Fig. 3 show that the NGICs have a clear imprint on the density profile of the ΛCDM halos. For the LN_p model the halos are not only more concentrated than the corresponding Gaussian-model halos, but they are also significantly cuspier. The opposite applies for the LN_n -model halos. In order to see in more detail the features of the inner density profiles of the halos, in Fig. 4 we show their slopes vs. the radius. Upper and lower panels are for the skew-positive and skew-negative statistics. In the left panels the two galaxy-sized halos

¹If the halo density profile flattens or even increases before attaining R_v , then the halo is truncated at the flattening radius. This happens only in some cases for subhalos or multiple halos. In most of the cases R_v is attained.

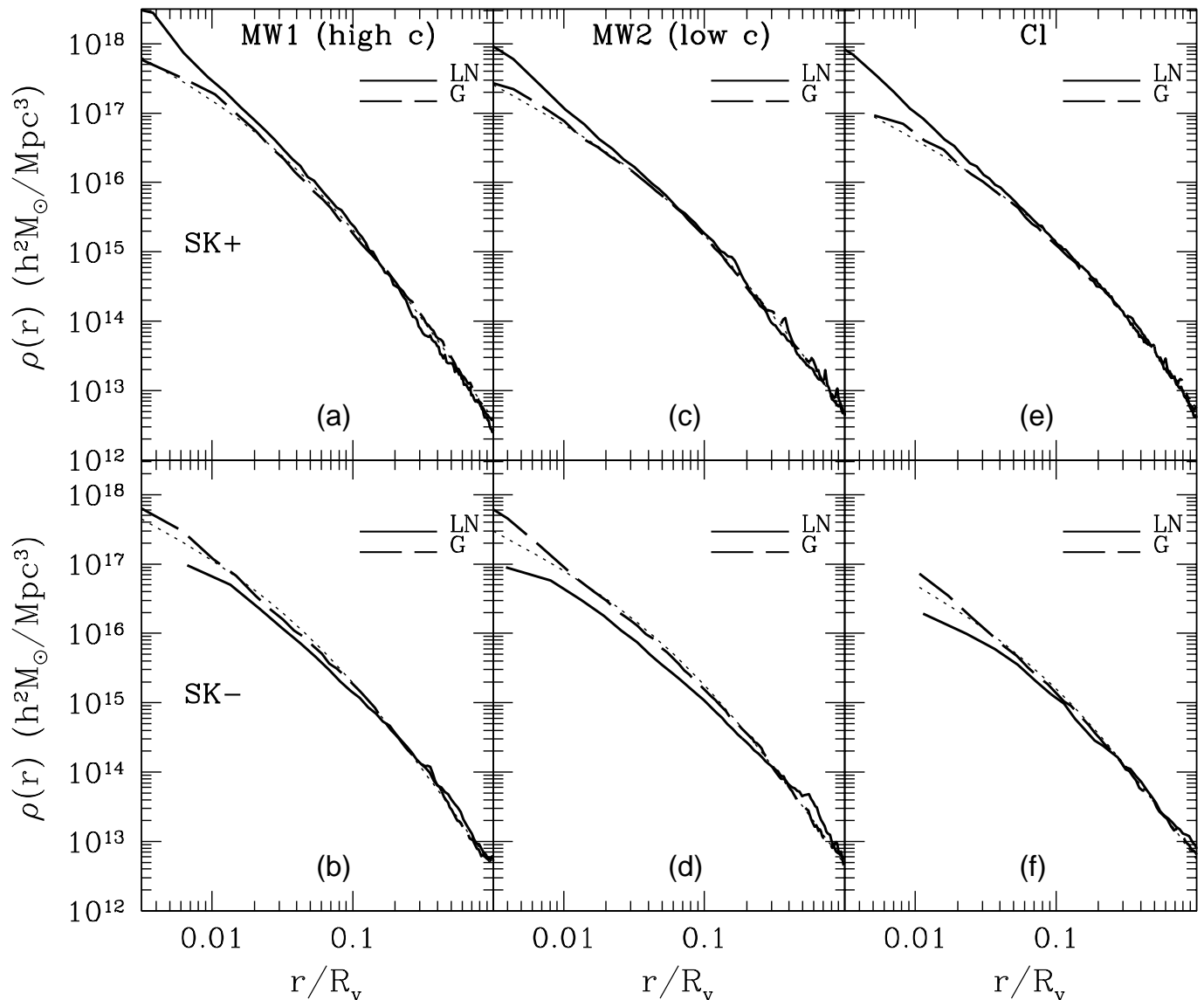


FIG. 3.— Density profiles of halos re-simulated with high resolution. Upper and lower panels are for the skew-positive and skew-negative statistics. The first and second columns are for the high- and low-concentration galaxy-sized halos, respectively, while the third column is for the only simulated cluster-sized halo. Solid lines are for the non-Gaussian halos and dashed lines are for the corresponding Gaussian counterpart (simulated with the same random seed). Dotted lines are the best NFW fitting to the Gaussian-halo density profiles. The LN_p (LN_n) halos are more (less) cuspy than the Gaussian counterpart halos.

are plotted (thick and thin lines are for the high and low concentration halos, respectively), while the right panels are for the cluster halo. As in Fig. 3, solid lines are for the non-Gaussian halos and dashed lines are for the corresponding Gaussian halos. In all the cases, the slopes of the non-Gaussian halos systematically depart from the slopes of the corresponding Gaussian halos at radii smaller than 3 – 10% the virial radius. The inner slopes of the LN_p (LN_n) halos are smaller (larger) than those of their corresponding Gaussian halos. Notice that the Gaussian halos corresponding to the LN_p run resulted with shallower profiles than the Gaussian halos corresponding to the LN_n run (this is part of the cosmic variance); the latter have

inner slopes around -1.4.

4.2. Spin Parameter and Angular Momentum Distribution

In Figure 5 we show the probability distribution of the modified spin parameter, $p(\lambda')$, for all halos from the $12.5 \text{ h}^{-1} \text{ Mpc}$ box with the different statistics; the G_n and G_p halos were joined into one denoted by G (see top-left panel). The parameter λ' determines the global angular momentum of a halo and it is defined as in Bullock et al. (2001):

$$\lambda' \equiv \frac{J_v}{\sqrt{2} M_v V_v R_v}, \quad (6)$$

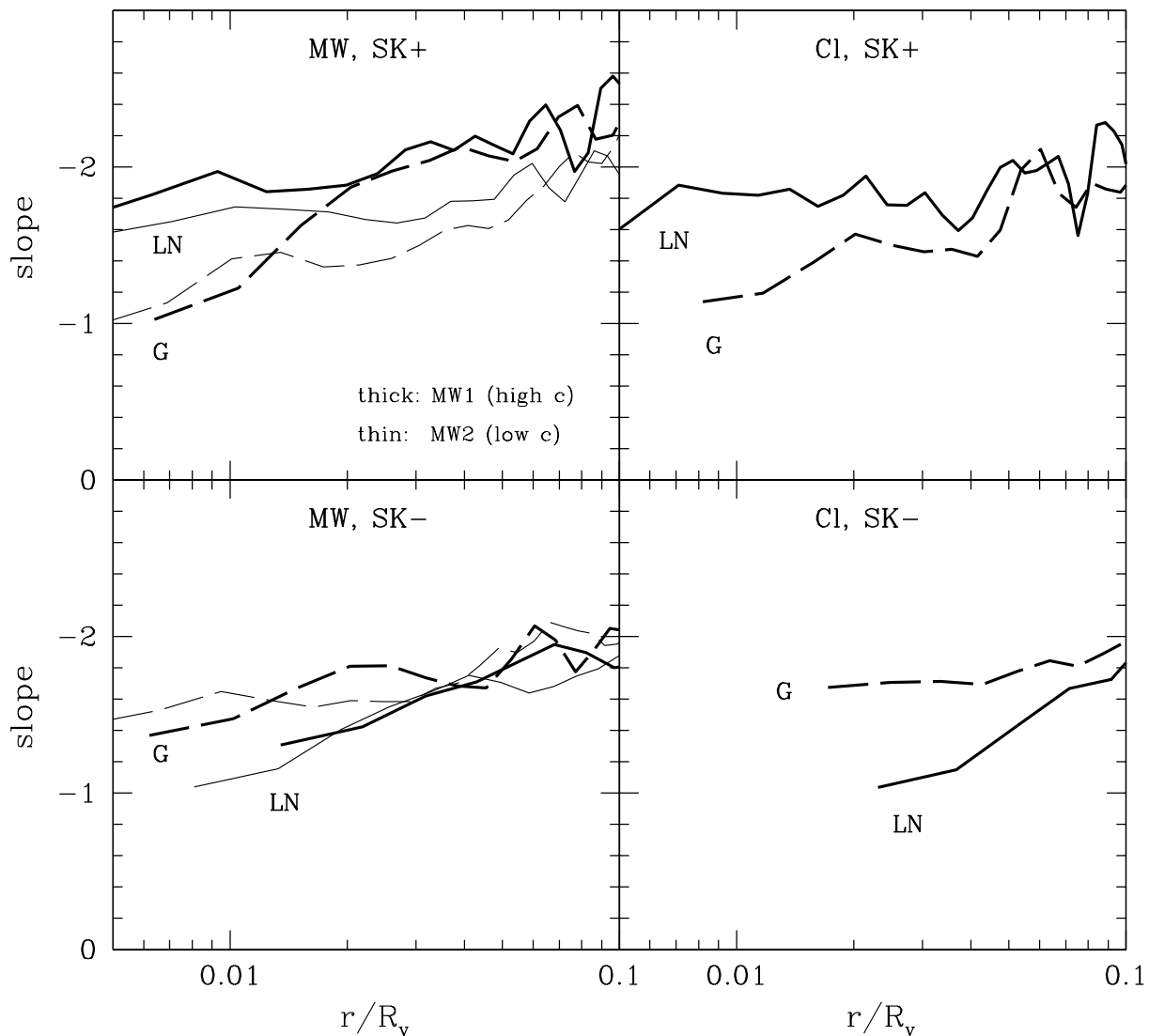


FIG. 4.— Density profile slopes in the inner parts of the non-Gaussian and Gaussian halos showed in Fig. 3. Upper and lower panels are for the skew-positive and skew-negative statistics. The two galaxy-sized halos are shown in the right panels (thick and thin lines for the high- and low-concentrated halo, respectively), while the cluster-sized halo is in the right panels. The line coding is the same than in Fig. 3.

where J_v is the angular momentum inside virial radius R_v , and V_v is the circular velocity at radius R_v . In Table 1, column (7), we show λ' for the high-resolution halos. The halo angular momentum is calculated as:

$$\mathbf{J} = m_i \sum_{i=1}^n \mathbf{r}_i \times \mathbf{v}_i, \quad (7)$$

where \mathbf{r}_i and \mathbf{v}_i are the position and velocity of the i th particle with respect to the halo center of mass.

The spin parameter distributions shown in Fig. 5 were obtained using halos with more than 100 particles. An extra simulation with 256^3 particles, with the same parameters as the $12.5 h^{-1} \text{Mpc}$ box simulation described in §3, was also run and stopped at $z = 1$. The about 1000 halos with more than 500 particles from this simulation were used to compute a well resolved LN_p spin-parameter

distribution (top-right panel). A complete analysis of this simulation has been deferred to a future paper. For Gaussian initial conditions, N -body simulations have shown previously that $p(\lambda')$ can be well described by the lognormal distribution (e.g., Bullock et al. 2001),

$$p(\lambda') = \frac{1}{\sigma_{\lambda'} \sqrt{2\pi}} \exp \left[-\frac{\ln^2(\lambda'/\lambda'_0)}{2\sigma_{\lambda'}^2} \right] \frac{d\lambda'}{\lambda'}. \quad (8)$$

We confirm this for our Gaussian simulations and find that the halo spin parameter distribution in a lognormal statistics (with positive or negative skewness) is also roughly lognormal. Curves on panels are the lognormal best-fits to the data: $(\sigma_{\lambda'}, \lambda'_0) = (0.63, 0.035)$, $(0.61, 0.029)$, $(0.73, 0.026)$, and $(0.49, 0.042)$ for Gaussian, LN_p (high resolution), and LN_p and LN_n (low resolution) simulations, respectively. The figure shows that halos formed in a LN_p statistics are biased to lower values of λ' ; on the contrary,

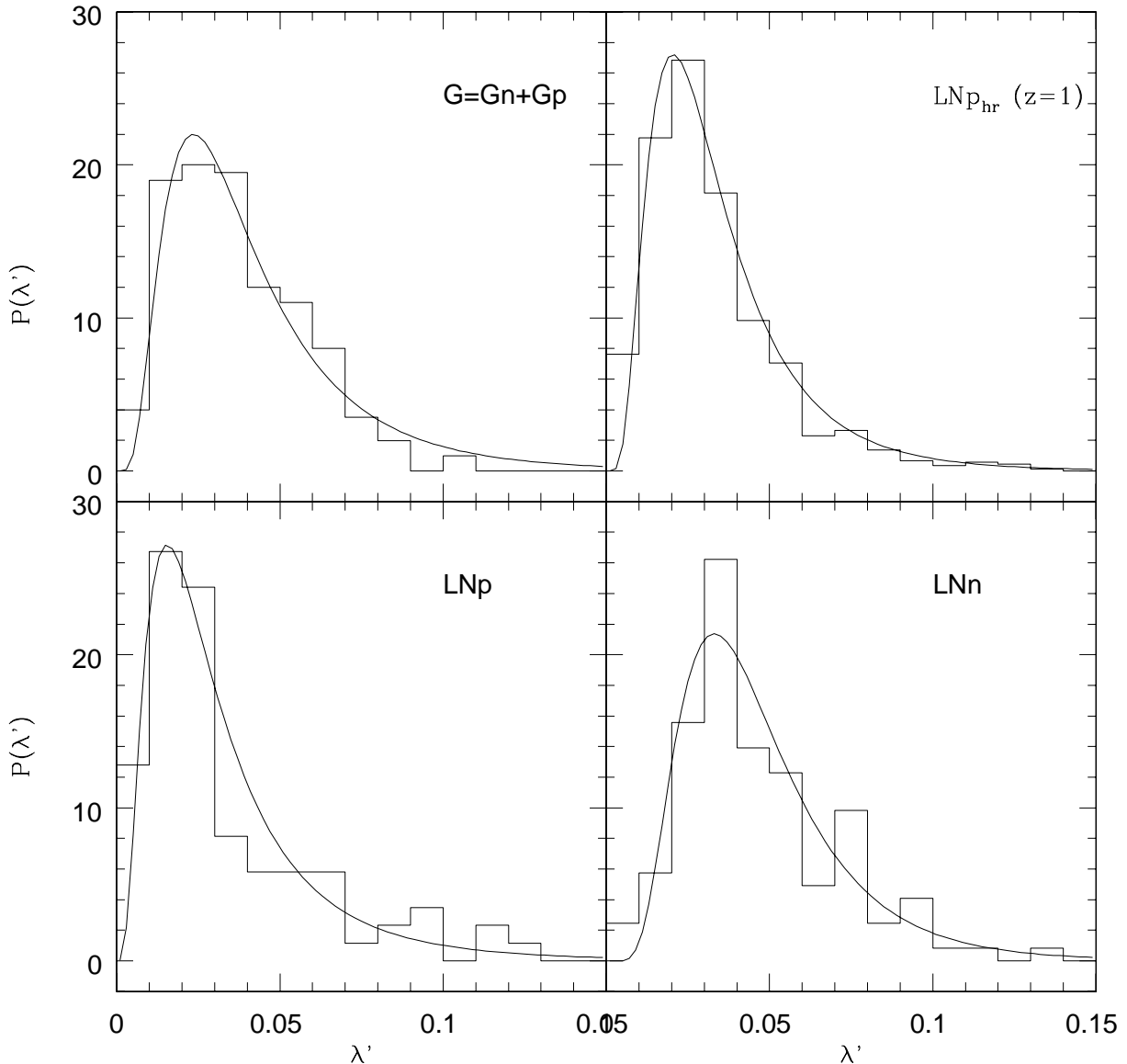


FIG. 5.— Probability distribution (histogram) of the halo spin parameter λ' for different statistics: Gaussian (top-left panel), skew-positive and negative lognormal from the low-resolution simulations (bottom panels), and skew-positive lognormal from a high-resolution simulation stopped at $z = 1$ (top-right panel). Curves on each panel are lognormal best-fits to the data. The λ'_0 parameter (see eq. [8]) in each curve is: 0.035 for the Gaussian (Gp and Gn added), 0.026 for LN_p (0.029 for the high resolution $z = 1$ simulation), and 0.042 for LN_n (the σ_λ parameter oscillates around 0.6, see text). As can be seen from the plot and confirmed by the λ'_0 values obtained from the fits, we find that LN_n (LN_p) halos have on average a higher (lower) λ' value than their Gaussian counterparts.

halos in the LN_n statistics seem to have on average a higher λ' value than their Gaussian counterparts.

For the halos re-simulated with high resolution, we compute also the halo angular momentum distribution (AMD). Figure 6 shows a comparison between the AMD of the galaxy-sized halos simulated with the skew-positive statistics, LN_p (left panels) and skew-negative, LN_n (right panels), and the AMD of each one of their Gaussian counterparts. The AMD is computed as follows. We find first, for each particle, the specific angular momentum component along \mathbf{J}_v , calling it j . We then divide the sphere of radius R_v in spherical shells and each of these shells is in

turn divided in four sections. Differences in the number of particles between cells for most of them are below a factor of two. The total j of any cell can be negative because j is a projected component. For each halo, we measured the mass fraction that there is in cells with negative j and found that it ranges from 5% to 50%. It is remarkable to find a halo (halo G2 $_{\text{Gp}}$) that, with the cell geometry adopted, happens to have about half of its cells pointing to the opposite direction of its total angular momentum. The calculation of the AMD proceeds only for those halos for which this fraction is small, less than $\sim 10\%$. Cells are ranked according to their j value (cells with negative j

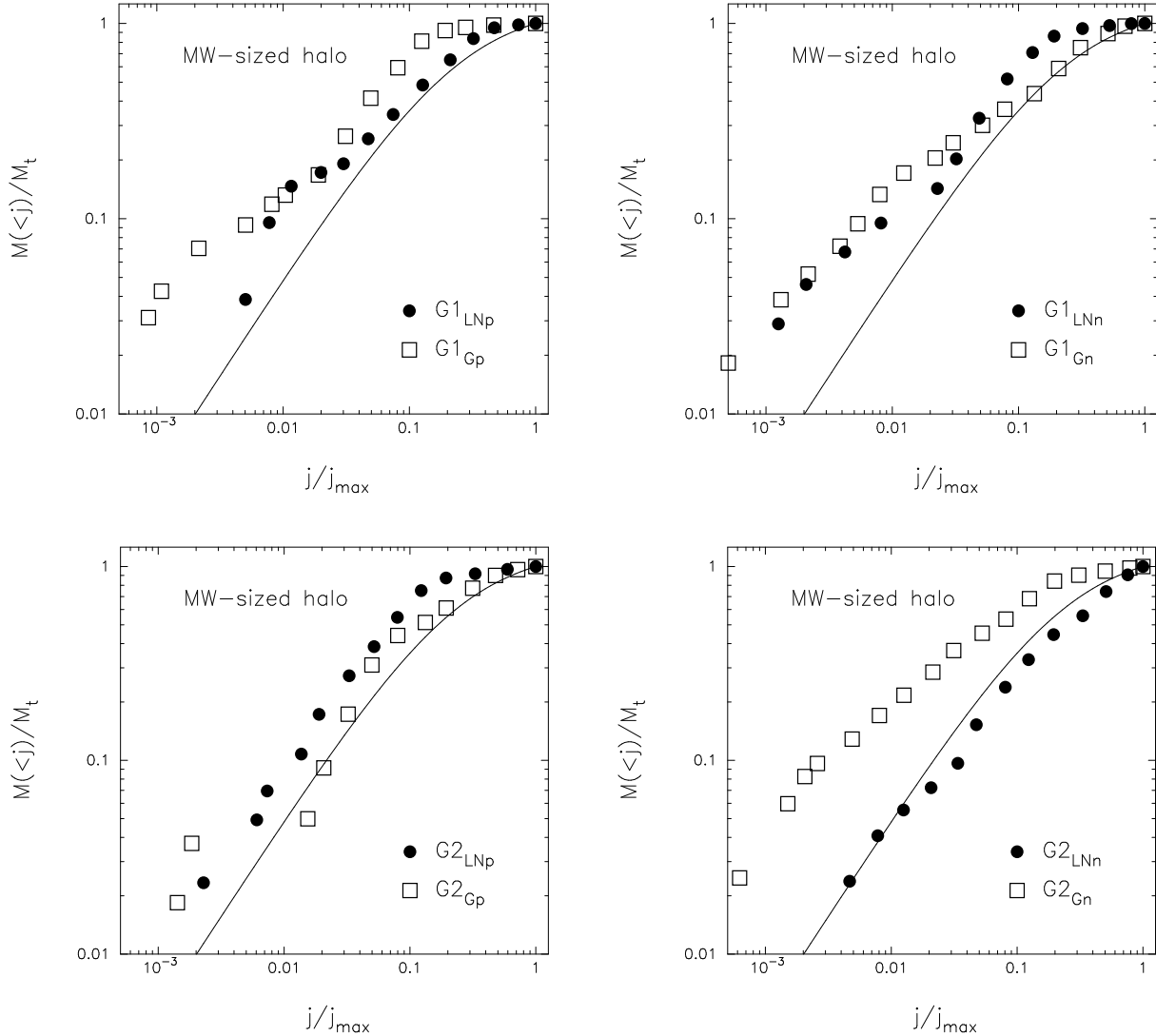


FIG. 6.— Specific angular momentum j distribution of halos G1 y G2 for the two lognormal statistics LN_p and LN_n , and their corresponding Gaussian realizations. Only cells with positive j were considered and the total mass M_t was redefined to be the mass contained only in those cells with positive j . The line is taken from the analytical fit of Bullock et al. (2001) $m(<j) = \mu \tilde{j} / (1 + \tilde{j})$, where $m(<j) \equiv M(<j) / M_{vir}$ and $\tilde{j} \equiv j / j_{max}$, with $\mu = 1.25$. No systematic differences are seen between halos simulated with lognormal NGICs and those simulated with the Gaussian statistics.

are rejected) and $M(<j)$ profiles are then built by counting the cumulative mass in cells with angular momentum smaller than j . Mass and angular momentum are given in M_v and j_{max} units, respectively, where j_{max} is the maximum value reached by j . We have also plotted in Figure 6 the analytical form of $M(<j)$ proposed by Bullock et al. (2001) with $\mu = 1.25$; the line is intended to guide the eye, it is not a fit to our numerical results.

4.3. Ellipticities

We have measured the ellipticities of halos using the tensor of inertia. This is defined as

$$I_{i,j} = \sum x_i x_j / r^2, \quad (9)$$

where the sum is over all particles within r_{vir} , x_i ($i = 1, 2, 3$) are the particle coordinates with respect to the halo

center of mass, and r is the distance of the particle to the halo center. The ellipticities are then given by

$$e_1 = 1 - \frac{\lambda_1}{\lambda_3}, \quad e_2 = 1 - \frac{\lambda_2}{\lambda_3}, \quad (10)$$

where $\lambda_3 > \lambda_2 > \lambda_1$ are the eigenvalues of the tensor of inertia. We evaluate the triaxiality parameter using the following formula (e.g., Franx, Illingworth, & de Zeeuw 1990)

$$T = \frac{\lambda_3^2 - \lambda_2^2}{\lambda_3^2 - \lambda_1^2}. \quad (11)$$

A halo is prolate (oblate) if $T = 1.0$ ($T = 0.0$).

The ellipticities e_1 (solid lines) and e_2 (dashed lines) as a function of radius are shown in Figure 7 for halos G2_{Gn} and G2_{LNp} (left panel) and for halos Cl_{Gp} and Cl_{LNp} (right panel). For these halos, no systematic difference is seen in ellipticities when using different statistics.

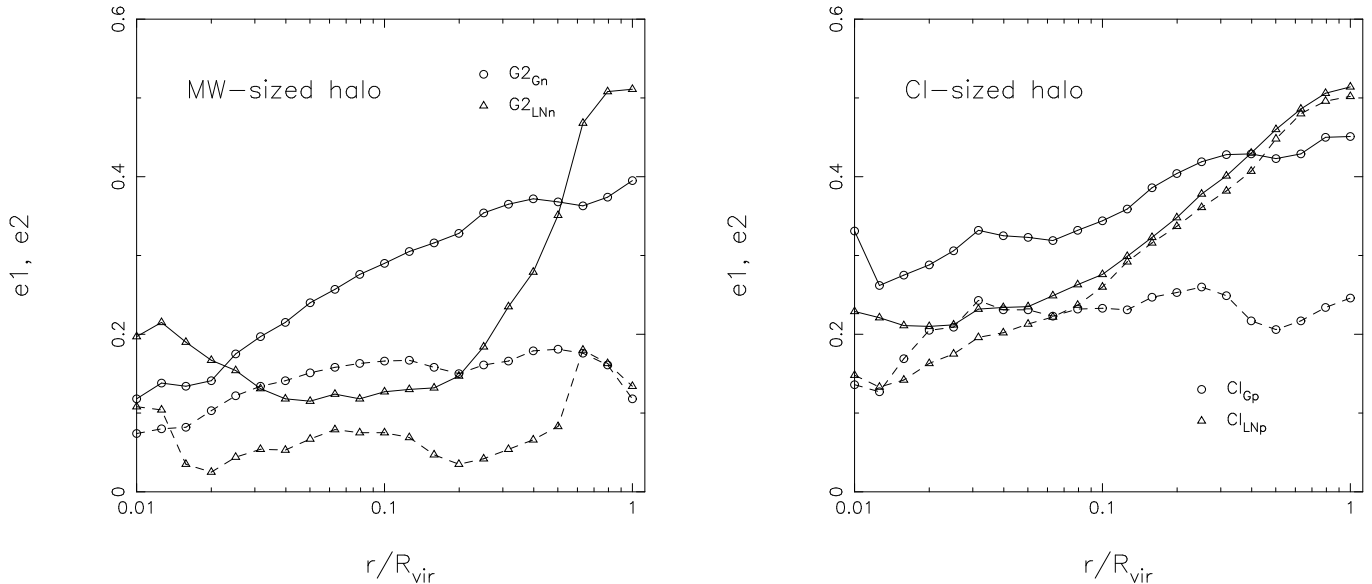


FIG. 7.— Ellipticities e_1 and e_2 as a function of radius are shown in left (halo G_2) and right (halo Cl) panels. By definition $e_1 < e_2$ and thus e_1 curves (dashed lines) lie below the corresponding e_2 curves (solid lines).

4.4. Subhalo Population

In Figure 8 we show the present-day subhalo v_{\max} cumulative function for all our galaxy-sized halos displayed in Table 1. All subhalos inside a radius of $200 \text{ h}^{-1} \text{ kpc}$ from the center of their parent halo are counted. We plot this function down to $v_{\max} \sim 20 \text{ kms}^{-1}$, where we believe we are complete (Klypin et al. 1999). The observational data (five pointed stars) are taken from Klypin et al. Two interesting and somewhat expected results come just from looking at the figure: substructure is suppressed in halos simulated with a LN_p statistics, as compared with the Gaussian one, while a slightly higher number of subhalos survive in the LN_n simulations. These results can be explained as an effect of the stronger (lighter) tidal field developed by their parent halos in the corresponding LN_p (LN_n) statistics (see §3.1 and Colín, Avila-Reese, & Valenzuela 2000).

5. SUMMARIZING DISCUSSION

We have analyzed the structure and substructure of Λ CDM halos obtained in low and high-resolution cosmological N -body simulations using non-Gaussian initial conditions (NGICs). The NGICs were generated in the gravitational potential with a lognormal statistics, positive-skewed (LN_p) in one case and negative-skewed (LN_n) in the other. The sign of the skewness remains the same when passing to the density PDF but the statistics are no longer lognormal. Since our aim is to explore in a generic way the influence of the NGICs on the properties of the halos, the particular choice of the NGICs is not relevant. In order to attain a fair comparison with results from the usual Gaussian-initial-conditions simulations, for each non-Gaussian simulation, we simulated the corresponding Gaussian one, using the same random seed. After the Zel'dovich approximation ($z = 50$), the skewnesses of the Gaussian, LN_p , and LN_n PDFs measured in the simula-

tions are 0.52, 3.90, and -1.27, respectively, while the G_3 parameter values are 3.05 and 0.067 for the LN_p and LN_n cases, respectively (for the Gaussian case $G_3 = 1$ by definition, see eq. [1]). These values are after some gravitational evolution, and they fall within the range of several of the theoretically proposed non-Gaussian statistics.

As discussed in the Introduction, the question of Gaussianity or not in the primordial fluctuation field is highly debated in theory as well as from the point of view of the observations. Most of the evidence shows that if the primordial fluctuation field is not-Gaussian, then the deviations from Gaussianity should not be very large. On the other hand, there is no reason to *a priori* conclude that the statistics is the same at all the scales. Most of the tests on Gaussianity were applied for relatively large scales (in the CMBR anisotropy maps and for cluster abundances). Even in this range of large scales, there have been some observational hints that the statistics could be different at different scales (e.g., Chiang et al. 2003). As far as we know, the present paper introduces for the first time a potential way to test Gaussianity at the smallest scales, using for this a comparison of the structure of galaxy and cluster-simulated halos with observational inferences.

Our main conclusion is that the structure and substructure of the galaxy- and cluster-sized Λ CDM halos are affected by the initial statistics. For the skew-positive (skew-negative) statistics, halos are more (less) concentrated, cuspiers (shallower), and with less (more) substructure than the corresponding Gaussian halo counterparts. These main findings are clearly seen in Figs. 2 and 3.

According to our results, the skew-positive NGICs would exacerbate the difficulty that the Gaussian Λ CDM model faces with observations: the rotation curves of dark-matter dominated (dwarf and low surface brightness) galaxies show that the inner density profiles of the halos are shallower and less concentrated than those of

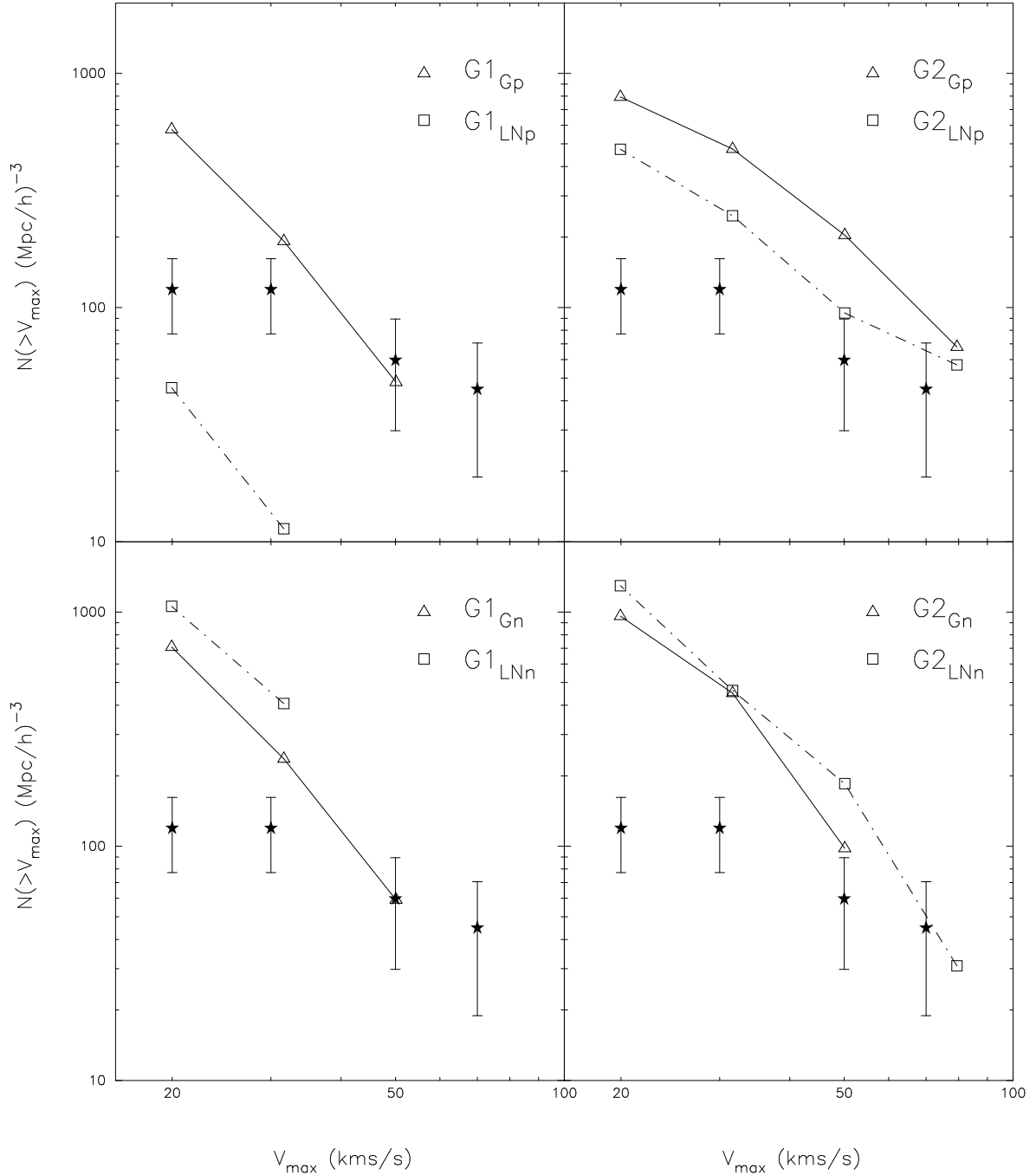


FIG. 8.— Cumulative subhalo v_{\max} -functions of halos G1 y G2 for the Gaussian and lognormal statistics. All subhalos with v_{\max} greater than 20 km s^{-1} within a sphere of radius $200 h^{-1} \text{ kpc}$ were counted. The averaged v_{\max} -function from satellites of the Milky Way and Andromeda is represented by stars (taken from Klypin et al. 1999). We plot for clarity only the error bars for the “observed” circular velocity function. It is clear that substructure is erased more efficiently in halos with a LN_p statistics than with a Gaussian one (see top panels). This effect can be traced back to the stronger tidal field experimented by subhalos in the LN_p scenario. The opposite effect is expected when the amount of substructure in a LN_n scenario is compared with its Gaussian counterpart. This is indeed the case: more subhalos survive under the LN_n statistics than under the Gaussian one.

the ΛCDM halos (see Colín et al. 2002 for references). We notice that tests related to cluster abundances and their evolution suggested skew-positive deviations from Gaussianity (see Introduction). On the other hand, the skew-negative NGICs work in the direction of making the

galaxy-sized dark halos less concentrated and shallower than the Gaussian ones.

Regarding the subhalo population, since the halos in the LN_p statistics are very concentrated, more subhalos are tidally destroyed than in the Gaussian case. The op-

posite occurs with the subhalo population in the LN_n simulations, although the difference with the Gaussian results in this case is very small. Observations show that the Gaussian Λ CDM model overpredicts the number of satellite subhalos within simulated galaxy-sized CDM halos (Klypin et al. 1999; Moore et al. 1999a). Nevertheless, this difference could be due to astrophysical processes (reionization, for example) which inhibit the formation of dwarf galaxies within the subhalos (Bullock, Kravtsov, & Weinberg 2000, Benson et al. 2002).

The halo spin parameter probability distribution also has shown to depend on the primordial statistics: LN_n (LN_p) halos have on average a higher (lower) λ' value than their Gaussian counterparts. A potential difficulty pointed out for the Gaussian halos is that the disks formed within them result too much concentrated (Navarro & White 1994). A possible way to improve on this problem is to generate halos with larger spin parameters than the Gaussian CDM ones. For example, this is the case for the LN_n model presented here.

From a theoretical point of view, our results raise an interesting problem: the density profile of the dark matter halos seems to depend on initial conditions. The question whether the structure of CDM halos is universal and non-dependent on cosmology, power spectrum, formation history, etc. has been several times discussed in the literature. Avila-Reese et al. (1998, 1999) have shown that the CDM halo density profiles oscillate around the NFW profile, depending mainly on the halo mass aggregation history (see also Wechsler et al. 2002). Nevertheless, a significant variation of the *inner* density profile was not expected, unless thermal processes are included, as is the case of self-interacting dark matter (e.g., Colín et al. 2002) or high rms-velocity dispersions due to thermal relicts (e.g., Avila-Reese et al. 1998, 2001; Lokas & Hoffmann 2000). It has been also shown that variations in the power spectrum shape and the type of the halo collapse (hierarchical merging or by fragmentation) do not introduce significant changes in the halo density profiles (Moore et al 1999b; Huss, Jain, Steinmetz 1999; Avila-Reese et al. 2001; Manrique et al. 2003). The fact that the initial statistics

of the fluctuation field does significantly affect the inner structure of the CDM halos is somewhat unexpected although, using the semi-numerical method of Avila-Reese et al. (1998), it was already shown that for a positive log-normal statistics (in the density field), the halos are more cuspy than in the Gaussian case (Viniegra 1997; Avila-Reese 1998). Halos form typically from the high-density peaks in the matter distribution. In the skew-positive statistics, high-density peaks are more abundant, isolated and “coherent” than in the Gaussian statistics; the opposite happens with the skew-negative statistics. The final structure of the halos is probably related to these facts. A deeper analysis of this question has been deferred to a future paper.

In the last few years, the observational determination of the cosmological parameters attained an unprecedented high accuracy and the body of astronomical observations of the local and high-redshift universe has grown dramatically. This progress not only allows to constrain better the cosmological models, but also opens a new dimension in the relaxation of some hypotheses made before, as well as in the exploration of second-order phenomena in the cosmic structure formation process. An example of this is just the statistics of the initial fluctuation field. Having now well defined the main cosmological parameters and a successful model of cosmic structure formation, one may explore the influence of NGICs on structure formation free of degeneracies with other parameters and assumptions (e.g., with Ω_m and σ_8).

We are grateful to Anatoly Klypin and Andrey Kravtsov for kindly providing us a copy of the ART code in its version of multiple mass, and for our enlightening discussions. PC is grateful to A. Kravtsov for providing access to a computer where the 256^3 -particle simulation was run. GP is grateful to Instituto de Astronomía, UNAM, for its kind hospitality during the development of this work. Part of the ART simulations were performed at the Dirección General de Servicios de Cómputo Académico, UNAM, using an Origin-2000 computer. This work was supported by CONACyT grants 33776-E to V.A. and 36584-E to P.C.

REFERENCES

- Acquaviva, V., Bartolo, N., Matarrese, S. & Riotto, A. 2002, *astro-ph/0209156*
- Allen, B., Caldwell, R.R., Dodelson, S., Knox, L., Shellard, E.P.S. & Stebbins, A. 1997, *Phys. Rev. Lett.*, 79, 2624
- Allen, T.J., Grinstein, B. & Wise, M.B. 1987, *Phys. Lett. B*, 197, 66
- Antoniadis, I., Mazur, P.O. & Mottola, E. 1997, *Phys. Rev. Lett.*, 79, 14
- Avelino, P.P., Shellard, E.P.S. & Wu, J.H.P. 1998, *ApJL*, 507, 101
- Avila-Reese, V., 1998, Ph.D. Thesis, Universidad Nacional Autónoma de México
- Avila-Reese, V., Firmani, C. & Hernández, X. 1998, *ApJ*, 505, 37
- Avila-Reese, V., Firmani, C., Klypin, A. & Kravtsov, A.V. 1999, *MNRAS*, 310, 527
- Avila-Reese, V., Colín, P., Valenzuela, O., D’Onghia, E., & Firmani, C. 2001, *ApJ*, 559, 516
- Banday, A.J., Zaroubi, S. & Górski, K.M. 2000, *ApJ*, 533, 575
- Barreiro, R.B., Hobson, M.P., Lasenby, A.N., Banday, A.J., Gorski, K.M. & Hinshaw, G. 2000, *MNRAS*, 318, 475
- Barrow, J.D. & Coles, P. 1990, *MNRAS*, 244, 188
- Bartolo, N., Matarrese, S. & Riotto, A. 2002, *Phys. Rev. D*, 65, 103505
- Benson, A.J., Frenk, C.S., Lacey, C.G., Baugh, C.M. & Cole, S. 2002, 333, 177
- Bernardeau, F. & Uzan, J. 2002, *Phys. Rev. D*, 65, 103506
- Bouchet, F.R., Peter, P., Riazuelo, A. & Sakellariadou, M. 2002, *Phys. Rev. D*, 65, 021301
- Bromley, B.C. & Tegmark, M. 2000, *ApJL*, 524, 79
- Bullock, J.S., Dekel, A., Kolatt, T.S., Kravtsov, A.V., Klypin, A.A., Porciani, C., & Primack, J.R. 2001, *ApJ*, 555, 240
- Bullock, J. S., Kravtsov, A.V., & Weinberg, D.H. 2000, *ApJ*, 539, 517
- Chiang, L-Y, Coles, P., & Naselsky, P. 2002, *MNRAS*, 337, 488
- Chiang, L-Y, Naselsky, P.D., Verkhodanov, O.V. & Way, M.J. 2003, *astro-ph/0303643*
- Chiu, W.A., Ostriker, J.P. & Staruss, M.A. 1998, *ApJ*, 494, 479
- Coles, P., Moscardini, L., Plionis, M., Lucchin, F., Matarrese, S. & Messina, A. 1993, *MNRAS*, 260, 572
- Colín, P., Avila-Reese, V., & Valenzuela, O. 2000, *ApJ*, 542, 622
- Colín, P., Avila-Reese, V., Valenzuela, O., & Firmani, C. 2002, *ApJ*, 581, 777
- Davé, R., Spergel, D.N., Steinhardt, P.J., & Wandelt, B.J. 2001, *ApJ*, 547, 574
- Durrer, R., Kunz, M. & Melchiorri, A. 1998, *Phys. Rev. D*, 59, 123005
- Einasto, J., et al. 1997, *Nature*, 385, 139
- Eke, V.R., Navarro, J.F., & Steinmetz, M. 2001, *ApJ*, 554, 114
- Ferreira, P.G., Magueijo, J. & Górski, K.M. 1998, *ApJL*, 503, 1
- Firmani, C. & Avila-Reese, V. 2003, in “Galaxy Evolution: Theory and Observations”, eds. V. Avila-Reese et al, *RevMexA&A (SC)*, 17, 109 (*astro-ph/0303543*)

- Franx, M., Illingworth, G., & de Zeeuw, T. 1990, *ApJ*, 383, 112
- Frenk, C.S. 2002, *Phil. Tran. Roy. Soc.*, 300, 1277 (astro-ph/0208219)
- Gangui, A., Martin, G. & Sakellariadou, M. 2002, *Phys. Rev. D*, 66, 083502
- Gaztañaga, E. & Baugh, C.M. 1998, *MNRAS*, 294, 229
- Gordon, C. & Lewis, A. 2002, astro-ph/0212248
- Gordon, C., Wands, D., Bassett, B. & Maartens, R. 2001, *Phys. Rev. D*, 63, 023506
- Huss, A., Jain, B., Steinmetz, M. 1999, *ApJ*, 517, 64
- Kamionkowski, M. 2003, in "Galaxy Evolution: Theory and Observations", Eds. V. Avila-Reese et al, *RevMexA&A (SC)*, 17, 1 (astro-ph/0209273)
- Klypin, A.A., Kravtsov, A.V., Valenzuela, O., Prada, F. 1999, *ApJ*, 522, 82
- Kravtsov, A.V., Klypin, A.A., & Khokhlov, A.M. 1997, *ApJS* 111, 73
- Klypin, A.A., Kravtsov, A.V., Bullock, J.S., & Primack, J.R. 2001, *ApJ*, 554, 903
- Klypin, A.A., & Holtzman, J., 1997, astro-ph/9712281
- Kofman, L.A. & Linde, A.D. 1987, *Nucl. Phys. B*, 282, 555
- Kogut, A., Banday, A.J., Bennett, C.L., Grski, K.M., Hinshaw, G., Smoot, G.F. & Wright, E.L. 1996, *ApJL*, 464, 29
- Komatsu, E. et al. 2003, astro-ph/0302223
- Koyama, K., Soda, J. & Taruya, A. 1999, *MNRAS*, 310, 1111
- Lesgourgues, J., Polarski, D. & Starobinsky, A.A. 1998, *MNRAS*, 297, 769
- Linde, A. & Mukhanov, V. 1997, *Phys. Rev. D*, 56, R535
- Lokas, E.L. & Hoffmann, Y. 2000, *ApJL*, 542, 139
- Lyth, D.H. & Wands, D. 2002, *Phys. Lett. B*, 524, 5
- Lyth, D.H., Ungarelli, C. & Wands, D. 2003, *Phys. Rev. D*, 67, 023503
- Magueijo, J. 2000, *ApJL*, 528, 57
- Manrique, A., Raig, A., Salvador-Solé, E., Sanchis, T. & Solanes J.M. 2003, *ApJ*, in press
- Martin, J., Riazuelo, A. & Sakellariadou, M. 2000 *Phys. Rev. D*, 61, 083518
- Matarrese, S., Ortolan, A. & Lucchin, F. 1989, *Phys. Rev. D*, 40, 290
- Matarrese, S., Lucchin, F., Messina, A. & Moscardini, L. 1991, *MNRAS*, 253, 35
- Messina, A., Moscardini, L., Lucchin, F. & Matarrese, S. 1990, *MNRAS*, 245, 244
- Moore, B., Ghigna, S., Governato, F., Lake, G., Quinn, T., Stadel, J., & Tozzi, P. 1999, *ApJ*, 524, L19
- Moore, B., Quinn, T., Governato, F., Stadel, J., & Lake, G. 1999, *MNRAS*, 310, 1147
- Moroi, T. & Takahashi, T. 2001, *Phys. Lett. B*, 522, 215
- Moroi, T. & Takahashi, T. 2002, *Phys. Rev. D*, 66, 063501
- Moscardini, L., Matarrese, S., Lucchin, F. & Messina, A. 1991, *MNRAS*, 248, 424 (MMLM)
- Navarro, J.F. & White, S.D.M. 1994, *MNRAS*, 267, 401
- Navarro, J.F., Frenk, C.S. & White, S.D.M. 1997, *ApJ*, 490, 493
- Ortolan, A., Lucchin, F. & Matarrese, S. 1988, *Phys. Rev. D*, 38, 465
- Pando, J., Valls-Gabaud D. & Fang L.Z. 1998, *Phys. Rev. Lett.*, 81, 4568
- Park, C.G., Park, C., Ratra, B., & Tegmark, M. 2001, *ApJ*, 556, 582
- Peacock, J.A. 1997, *MNRAS*, 284, 885
- Peebles, P.J.E. 1999, *ApJ*, 510, 523
- Peiris, H.V. et al. 2003, astro-ph/0302225
- Pen, U., Seljak, U. & Turok, N. 1997, *Phys. Rev. Lett.*, 79, 1611
- Polenta, G. et al. 2002, *ApJL*, 572, 27
- Robinson, J. & Baker, J.E. 2000, *MNRAS*, 311, 781
- Robinson, J., Gawiser, E. & Silk, J. 2000, *ApJ*, 532, 1
- Salopek, D.S. 1992, *Phys. Rev. D*, 45, 1139
- Santos, A. et al. 2002, *Phys. Rev. Lett.*, 88, 241302
- Sakellariadou, M. 2002, Proceedings of NATO ASI / COSLAB (ESF) School "Patterns of symmetry breaking", hep-ph/0212365
- Szapudi, I. et al. 2002, *ApJ*, 570, 75
- Tegmark, M., de Oliveira-Costa, A. & Hamilton, A. 2003, astro-ph/0302496
- Turok, N. & Spergel, D. 1990, *Phys. Rev. Lett.*, 64, 2736
- Verde, L. 2000, *Annals of The New York Academy of Sciences*, Vol. 927, p. 54 (astro-ph/0004341)
- Verde, L., Wang, L., Heavens, A & Kamionkowski, M. 2000, *MNRAS*, 313, 141
- Verde, L., Kamionkowski, M., Mohr, J.J. & Benson, A.J. 2001, *MNRAS*, 321, L7
- Verde, L., Jimenez, R., Kamionkowski, M. & Matarrese, S. 2001a, *MNRAS*, 325, 412
- Verde, L. et al. 2002, *MNRAS*, 335, 432
- Viniegra, F. 1997, B.Sc. Thesis, Universidad Nacional Autónoma de México
- Wechsler, R.H., Bullock, J.S., Primack, J.R., Kravtsov, A.V. & Dekel, A. 2002, *ApJ*, 568, 52
- Weinberg, D.H. & Cole, S. 1992, *MNRAS*, 259, 652
- Willick, J.A. 2000, *ApJ*, 530, 80
- Wu, J.H.P. et al. 2001, *Phys. Rev. Lett.*, 87, 251303